Acta Crystallographica Section A
Foundations of Crystallography
ISSN 0108-7673

Received 9 August 2010
Accepted 21 December 2010

Form, symmetry and packing of biomacromolecules. III. Antigenic, receptor and contact binding sites in picornaviruses

A. Janner

Theoretical Physics, FNWI, Radboud University, Heyendaalseweg 135, NL-6525 AJ Nijmegen, The Netherlands. Correspondence e-mail: a.janner@science.ru.nl

The relation between serotype differentiation and crystallographic symmetry, revealed by the contact fingerprint diagrams investigated in Part II [Janner (2010). *Acta Cryst.* A**66**, 312–326] for the human rhinovirus, is extended to the *Picornaviridae* family. The approach, outlined in Part I [Janner (2010). *Acta Cryst.* A**66**, 301–311] and Part II for biomacromolecules packed in a crystal and based on concepts such as packing lattice, kissing points and crystal-packing parameters, can directly be applied to the picornaviruses. In particular, the contact fingerprint diagrams of 20 different virus strains have been derived. In these cases, as for the rhinovirus, these diagrams are serotype/strain specific, justifying the name fingerprint. The molecular basis for the serotype variability, and the associated conservation requirements, is usually analysed by considering antigenic sites, where capsid residues bind with antibodies, and receptor sites, where other residues bind with molecular receptors of the host cell membrane. Both the antigenic variation and the receptor conservation allow repeated infection of the host cells of the given animals. The graphical description of these sites is usually done by footprints and roadmap diagrams, mapping properties of the capsid surface and using the icosahedral symmetry of the capsid. The alternative fingerprint diagrammatic description, based on the crystal symmetry, adopted in Part II for the contact sites, where a capsid is bound to the next one in the crystal packing, is extended to the antigenic and receptor binding sites. Again, the antigenic/receptor fingerprints are specific, at least for the nine picornaviruses investigated so far, despite the more than a factor of ten larger coarse graining with respect to the corresponding footprint and roadmap diagrams. The latter are based on a grid spacing of about 2 Å, whereas the spacing implied by the packing-lattice approximation adopted in fingerprints varies typically from 20 to 50 Å. The fingerprint diagrams are accordingly simpler (because approximated), but nevertheless still serotype specific, despite the complex character of the interactions involved.

1. Introduction

The peculiar crystallographic properties of single biomacromolecules revealed by enclosing forms with vertices at projected points of a lattice, the *molecular form lattice*, which connects external surfaces with internal ones (like those of central holes), allow a characterization of the conserved architecture of icosahedral rhinoviruses (Janner, 2006*a*). In particular, clusters of amino acids with an axial symmetry (decamers, pentamers, hexamers, trimers and tetramers) occurring in the coat proteins VP1, VP2, VP3 and VP4 of the viral capsid have symmetry-dependent crystallographic forms which are serotype independent.

The structural basis of the serotype dependency appears when considering single crystals of rhinoviruses as packed virions. This is discussed in Part II (Janner, 2010*b*) in a similar way as in Part I (Janner, 2010*a*), where crystal lattice and form lattice are related by a *packing lattice*. For icosahedral viruses one naturally also considers packing of equal spheres and their contact points (the *kissing points*).

The first aim of this paper, Part III, is the test of the validity of the approach for the larger viral family of the *Picornaviridae*, to which the rhinoviruses belong. This choice is not only justified by the large economical and biochemical impact of the picornaviruses, but also because a great variability is combined with conserved common structural elements. It is, therefore, not surprising to find a very large number of articles devoted to these properties, as reported in the book of Semler & Wimmer (2002). Within this huge amount of papers, one finds crystal-packing considerations, but not the molecular

Table 1
Picornaviruses (a selection).

Genus and name	Serotype and strain	PDB key	Space group	Primary citation
I. *Aphthovirus*				
Foot-and-mouth disease virus (FMDV)	O1	1BBT	$I23$	Fry *et al.* (1993)
	A 1061	1ZBE	$H3$	Fry *et al.* (2005)
	C	1FMD	$I23$	Lea *et al.* (1994)
II. *Enterovirus*				
Human poliovirus	Type 1	2PLV	$P2_12_12$	Filman *et al.* (1989)
	Type 2	1EAH	$C222_1$	Lentz *et al.* (1997)
	Type 3	1PVC	$I222$	Filman *et al.* (1989)
Coxsackievirus	A21	1Z7S	$P4_232$	Xiao *et al.* (2005)
	B3	1COV	$P2_1$	Muckelbauer *et al.* (1995)
Swine vesicular disease virus (SVDV)	(∼B5)	1MQT	$I222$	Verdaguer *et al.* (2003)
	ukg/27/72	1OOP	$P22_12_1$	Fry *et al.* (2003)
Echovirus 1	EV1	1EV1	$P2_12_12$	Filman *et al.* (1998)
Echovirus 11	EV11	1H8T	$H32$	Stuart *et al.* (2002)
III. *Rhinovirus*				
Human rhinovirus (HRV)	HRV16	1AYM	$P22_12_1$	Hadfield *et al.* (1997)
	HRV14	4RHV	$P2_13$	Arnold & Rossmann (1990)
	HRV3	1RHI	$P2_122_1$	Zhao *et al.* (1996)
	HRV2	1FPN	$I222$	Verdaguer *et al.* (2000)
	HRV1A	1R1A	$P6_322$	Kim *et al.* (1989)
IV. *Cardiovirus*				
Mengo encephalomyelitis virus		2MEV	$P2_12_12_1$	Krishnaswamy & Rossmann (1990)
Theiler murine encephalomyelitis virus	DA	1TME	$P2_12_12$	Grant *et al.* (1992)
	BeAn	1TMF	$P4_322$	Luo *et al.* (1992)

crystallographic component that characterizes the present approach. References, directly related to aspects discussed in this paper, can be found in the subsequent sections.

The second aim is to express in the new way variability and conservation, which are essential properties of viruses, as an alternative to the normal approach.

To survive and reproduce, a virus has to conserve the ability to infect a given sort of cells. Cell attachment, a first stage in this process, takes place by binding the virion to specific cell membrane proteins, the cellular receptors. One finds the *receptor binding sites* at the external surface of the capsid.

The defence against infection is ensured by the immune system, which recognizes foreign macromolecules, known as antigens, and generates antibodies that bind to the virus at *antigenic sites*, again at the external surface of the capsid, neutralizing, in most cases, the ability of the virus to infect the cell. In reality, the whole mechanism of the immune response is more complex and a full description is outside the scope of this paper; however, the essential features are the ones mentioned.

The key point is that a virion has to conserve the structure of the receptor sites, while changing that of the antigenic sites in order to escape the action of the immune defence. Antigenic variation permits a virus to reinfect its host. The molecular basis of the serotype differentiation is mainly determined by the antigenic sites at exposed regions of the capsid surface, in competition with neighbouring receptor sites.

Viral *contact sites*, where one virus binds to the next one giving rise to the crystal packing, also occur at exposed regions of the external surface of the capsid, as is the case for the antigenic and receptor binding sites. It is, therefore, not surprising to find a connection between serotype and contact sites, as discussed in Part II.

A first step towards an understanding of the possible mutual relations between these different binding sites requires a common description. In the present approach the common elements are based on the space-group symmetry of the crystal and not on the icosahedral symmetry of the capsid in order to understand better the space-group variability (Janner, 2010*b*), as opposed to the conserved enclosing forms observed in the rhinoviruses (Janner, 2006*a*).

Adopting the *Picornaviridae* family as a field of investigation allows one to combine a desired generality with the necessary limitations.

2. The *Picornaviridae* family

Picornaviruses are small (pico) RNA animal viruses with icosahedral symmetry of the capsid, which is built from three major coat proteins (VP1, VP2, VP3) sharing a conserved core of a wedge-shaped, eight-stranded antiparallel beta-barrel motif. A fourth coat protein (VP4) lies more inside the capsid and ensures contact with the single-stranded RNA genome. The enclosing form of the capsid is an ico-dodecahedron (Janner, 2006*b*), which in the Caspar–Klug classification corresponds to a pseudo $T = 3$ arrangement of the major capsid proteins. Depending on the virus species, the roughly spherical capsid shows more or less pronounced protruding chain segments and depressions formed by clefts in the surface, giving rise to typical structures like the so-called 'canyon' considered by Rossmann & Palmenberg (1988) and Rossmann (1989).

The picorna family is currently subdivided into nine genera: *Aphthovirus*, *Enterovirus*, *Rhinovirus*, *Cardiovirus*, *Hepatovirus*, *Parechovirus*, *Erbovirus*, *Kobuvirus* and *Teschovirus* (Semler & Wimmer, 2002). Considered here is a selection of picornaviruses, listed in Table 1, whose structural data, determined by X-ray diffraction, have been deposited in the Protein Data Bank (PDB). They all belong to the first four genera indicated above. More details can be found at the VIPER website (http://viperdb.scripps.edu).

Despite their similar architecture, picornaviruses show a great variability in their specific properties. For example, rhinoviruses occur in more than 100 serotypes, making it practically impossible to develop vaccines against them, whereas the poliovirus can be assigned to one of three serotypes; seven serotypes are known for the foot-and-mouth

Table 2
Crystal packing of picornaviruses.

PDB key	Virus name and serotype	Crystal space group	Bravais lattice of Λ_P	Packing parameters						
				k	N_a	N_b	N_c	n_a	n_b	n_c
1BBT	FMDV O 1	$I23$	$23P$	8	12	12	12	5	5	5
1ZBE	FMDV A 1061	$H3$	$3H$	12	6	6	24	3	3	5
1FMD	FMDV C	$I23$	$23P$	8	12	12	12	5	5	5
2PLV	Polio 1	$P2_12_12$	$222P$	8	8	12	12	4	5	5
1EAH	Polio 2	$C222_1$	$222P$	8	16	16	16	7	5	5
1PVC	Polio 3	$I222$	$222P$	8	10	14	10	5	6	4
1Z7S	Coxsackie A21	$P4_232$	$432P$	8	16	16	16	7	7	7
1COV	Coxsackie B3	$P2_1$	$2P$	10	16	8	16	4	4	5
1MQT	Swine (∼B5)	$I222$	$222P$	8	12	14	10	6	6	4
1OOP	Swine ukg/27/72	$P22_12_1$	$222P$	8	12	12	24	5	5	11
1EV1	Echo type 1	$P2_12_12$	$222P$	4	12	12	16	4	4	7
1H8T	Echo type 11	$H32$	$32H$	12	6	6	48	3	3	5
1AYM	Rhinovirus 16	$P22_12_1$	$222P$	8	12	12	16	5	5	7
4RHV	Rhinovirus 14	$P2_13$	$23P$	12	12	12	12	4	4	4
1RHI	Rhinovirus 3	$P2_122_1$	$222P$	8	16	16	12	6	7	6
1FPN	Rhinovirus 2	$I222$	$222P$	8	10	14	10	5	6	4
1R1A	Rhinovirus 1A	$P6_322$	$622P$	6	12	12	12	6	6	4
2MEV	Mengo	$P2_12_12_1$	$222P$	12	8	8	8	3	3	3
1TME	Theiler DA	$P2_12_12$	$222P$	8	16	20	16	7	9	7
1TMF	Theiler BeAn	$P4_322$	$432P$	12	8	8	16	4	4	3

disease virus and the swine vesicular disease viruses all belong to a single serotype (Verdaguer *et al.*, 2003).

3. Crystal packing and packing lattices

In Part II the serotype variability of rhinoviruses has been analysed in terms of packing lattices, contact residues and fingerprint diagrams. The concept of packing lattice, defined and applied in Part I, allows one to bridge the gap between the crystallographic properties of individual biomacromolecules, characterized by a molecular form lattice, and their symmetry when periodically packed as a crystal.

The application of this approach to the larger family of picornaviruses is, more or less, straightforward and leads to similar characterizations as for rhinoviruses, summarized here in Table 2 for the 20 species listed in Table 1. The packing parameters reported in Table 2 have the meaning already introduced in Parts I and II: k is the kissing number of the sphere packing, the integers N_a, N_b, N_c relate the lattice parameters a, b, c of the crystal with the ones u, v, w of the packing lattice Λ_P:

$$a = N_a u, \quad b = N_b v, \quad c = N_c w \tag{1}$$

and the integers n_a, n_b, n_c define an enclosing form of the virion with vertices at points of the lattice Λ_P. In the ideal case, these parameters satisfy the relation

$$R_0 = n_a u = n_b v = n_c w, \tag{2}$$

with R_0 the radius of a sphere enclosing the capsid. In this ideal case the ratios of the lattice parameters are rational numbers given by

$$\frac{a}{b} = \frac{N_a n_b}{N_b n_a}, \quad \frac{b}{c} = \frac{N_b n_c}{N_c n_b}, \quad \frac{a}{c} = \frac{N_a n_c}{N_c n_a}, \tag{3}$$

and

$$\frac{u}{v} = \frac{n_b}{n_a}, \quad \frac{v}{w} = \frac{n_c}{n_b}, \quad \frac{u}{w} = \frac{n_c}{n_a}. \tag{4}$$

The rational values of these ratios ensure in the hexagonal, tetragonal and orthorhombic cases that the corresponding lattices are integral (Janner, 2004). The cubic case is always integral and in the monoclinic or triclinic cases additional angular relations are required.

Instead of deriving these relations for the orthorhombic case with the twofold axes aligned with the icosahedral ones of the capsid (as done in Part II), we assume here their validity for what is denoted as the ideal case.

A real crystal is always an approximation of a corresponding ideal one. In the present case this is in particular true for the description of the crystal as packed spheres and for the packing lattice, which we recall is not unique. It is, therefore, important to make the deviations between ideal and real structure as transparent as possible. The graphical rendering adopted for the packed crystal structures already gives an overall view of the relative importance of these deviations. In addition, the numerical values of the ratios of the lattice parameters reported in Table 3 permit a quantification of the difference between ideal and real.

In what follows some illustrative examples are presented. The corresponding figures for the rhinoviruses have already been published in Part II. Before doing so, it is advisable to explain again the difference between the concept of molecular form lattice Λ_M, already applied to many biomacromolecules [see, in particular, Janner (2008) and references therein], and the concept of packing lattice Λ_P introduced in Part I.

3.1. On the difference between molecular form lattice and packing lattice

Let us first discuss the molecular form lattice. A molecule is three dimensional and discrete. Its Euclidean symmetry is

Table 3
Parameters and relations of picornaviruses.

			Crystal lattice Λ					Packing lattice Λ_P		
			Parameters (Å)			Ideal ratios and experimental value		Parameters (Å)		
PDB key	Virus name and serotype	Size R_0 (Å)	*a*	*b*	*c*	*a*/*b*	*a*/*c*	*u*	*v*	*w*
1BBT	FMDV O1	147.2	345.00	345.00	345.00	1	1	29	29	29
1ZBE	FMDV A	148.8	306.20	306.20	712.80	1	$\frac{5}{12} \simeq 0.416$ (0.429)	51	51	30
1FMD	FMDV C	147.2	347.60	347.60	347.60	1	1	29	29	29
2PLV	Polio 1	153.7	322.94	358.04	380.15	$\frac{5}{6} \simeq 0.833$ (0.902)	$\frac{5}{6} \simeq 0.833$ (0.849)	40	30	32
1EAH	Polio 2	153.7	345.70	497.20	485.90	$\frac{5}{7} \simeq 0.714$ (0.695)	$\frac{5}{7} \simeq 0.714$ (0.714)	22	31	30
1PVC	Polio 3	153.7	321.06	358.62	381.82	$\frac{6}{7} \simeq 0.857$ (0.895)	$\frac{4}{5} \simeq 0.8$ (0.841)	32	26	38
1Z7S	Coxsackie A21	151.3	348.01	348.01	348.01	1	1	22	22	22
1COV	Coxsackie B3	151.3	574.62	302.07	521.61	2 (1.902)	$\frac{5}{4} \simeq 1.25$ (1.102)	36	38	33
1MQT	Swine (∼B5)	148.8	318.35	349.96	371.72	$\frac{6}{7} \simeq 0.857$ (0.909)	$\frac{4}{5} \simeq 0.8$ (0.856)	27	25	37
1OOP	Swine ukg/27/72	147.2	354.10	371.70	318.60	1 (0.952)	$\frac{11}{10} \simeq 1.1$ (1.111)	29	31	13
1EV1	Echo type 1	156.9	472.15	483.20	352.45	1 (0.977)	$\frac{21}{16} \simeq 1.312$ (1.340)	39	40	22
1H8T	Echo type 11	160.2	300.85	300.85	1476.62	1	$\frac{5}{24} \simeq 0.208$ (0.204)	50	50	31
1AYM	Rhinovirus 16	147.2	362.60	347.10	334.90	1 (1.044)	$\frac{21}{20} \simeq 1.05$ (1.082)	30	29	21
4RHV	Rhinovirus 14	147.2	445.10	445.10	445.10	1	1	37	37	37
1RHI	Rhinovirus 3	153.7	397.90	341.80	301.70	$\frac{7}{6} \simeq 1.166$ (1.164)	$\frac{4}{3} \simeq 1.333$ (1.319)	25	21	25
1FPN	Rhinovirus 2	153.7	308.68	352.98	380.48	$\frac{6}{7} \simeq 0.857$ (0.874)	$\frac{4}{5} \simeq 0.8$ (0.811)	31	25	38
1R1A	Rhinovirus 1A	150.5	341.30	341.30	465.90	1	$\frac{2}{3} \simeq 0.666$ (0.732)	28	28	38
2MEV	Mengo	153.7	441.42	427.31	421.92	1 (1.033)	1 (1.046)	55	53	53
1TME	Theiler DA	156.9	360.50	338.40	348.10	$\frac{36}{35} \simeq 1.028$ (1.065)	1 (1.035)	23	17	22
1TMF	Theiler BeAn	161.8	331.86	331.86	796.26	1	$\frac{3}{8} \simeq 0.375$ (0.416)	41	41	50

always a point group of finite order which, in general, is non-crystallographic. This means that it does not leave invariant a lattice of the same dimension. There is, however, always an *N*-dimensional lattice left invariant by the point group of the molecule (more precisely, by a point group isomorphic to that of the molecule). Consider a polyhedral form enclosing the given molecule and having the same point-group symmetry. The vertices of this form can be obtained from the projection in three dimensions of points of the *N*-dimensional lattice Λ_M considered above. Accordingly, these vertices can be indexed by a set of *N* integral indices, which are the lattice coordinates of the corresponding lattice point of Λ_M. This is the reason why this lattice is denoted as the molecular form lattice. The projected lattice points do not form a lattice (in general they do not form a discrete set in three dimensions), but are elements of what is denoted as a *Z*-module of dimension 3 and rank *N*. The value of *N* depends on the point group: it is 4 for a planar pentagonal point group, 6 for an icosahedral one and 3 for a cubic point group.

Consider now the packing lattice and the crystal of a given molecule described as a packing of (equal) spheres. In this description the molecule is replaced by its spherical enclosing form. The symmetry of a sphere is non-crystallographic, but not being a finite group, there are no invariant lattices for any finite dimension *N*. Therefore, the concept of molecular form lattice is not applicable. It is possible, however, to consider a three-dimensional lattice Λ_P, left invariant by the space group of the crystal and fine enough to approximate points belonging to the spherical enclosing forms. Therefore, the crystal lattice Λ is a sublattice of Λ_P. This leads to equation (1), which relates the lattice parameters *a*, *b*, *c* of Λ with those *u*, *v*, *w* of Λ_P. One requires, moreover, that the kissing points of the packing (where spheres touch) and the centres of the spheres are at points of Λ_P. Then Λ_P is denoted as a packing lattice. It is clear that for a given crystal a packing lattice is an approximation and never unique. Whereas Λ_M is symmetry adapted to a single molecule (left invariant by the point group of the molecule) and *N* dimensional, Λ_P is symmetry adapted to the lattice periodic arrangement of these molecules (left invariant by the space group) and three dimensional. So far the two concepts are independent.

The situation becomes more subtle when, in the crystal packing, the molecule is replaced by enclosing forms having the molecular point-group symmetry. Again, the packing lattice considered should approximate well enough points of the enclosing form, and the polyhedral vertices in particular. This implies that the packing lattice appears as an approximation of the projected lattice points of Λ_M which are morphologically relevant. In particular, for the icosahedral viruses this situation is likely to occur for spherical enclosing forms inscribed in the molecular ones having icosahedral symmetry. In this respect, the two lattices are no longer independent and reflect the approximate compatibility between molecular and crystallographic point-group symmetries. For all these reasons, in the crystal-packing figures one finds in the paper, the crystal unit cell is given together with the lattice points of Λ_P and with examples of the two types of packing units, the spherical and/or the polyhedral ones enclosing the coat proteins of the capsid, also indicated.

In Part I, where the concept of packing lattice was introduced, the explanation of the difference between packing lattice and molecular form lattice has not been based on the simpler case of packing of spheres, because the primary goal of Part I was the elucidation of the relation between the crystallography of single molecules and that of their crystals. This

required consideration of the packing of indexed molecular forms and not of spherical ones.

3.2. The mengovirus

The mengovirus (PDB refcode 2MEV; Krishnaswamy & Rossmann, 1990) is the first simple example of a spherical packing obtained by applying the crystal space group $P2_12_12_1$ to the capsid centred at the origin [Wyckoff position 4(a) with $x = y = z = 0$] and icosahedral twofold axes aligned with the orthorhombic ones (Fig. 1). The 12 kissing points are at the same position 4(a): four with $x = y = 1/4, z = 0$, four with $x = z = 1/4, y = 0$ and four with $y = z = 1/4, x = 0$. In this case $N_a = N_b = N_c = 8$ and $n_a = n_b = n_c = 3$, so that the ideal lattice is cubic. The real one shows small deviations from the cubic ratios 1 ($a/b = 1.033$, $b/c = 1.028$, $a/c = 1.046$).

3.3. The echovirus type 1

This case (1EV1; Filman *et al.*, 1998) has been chosen because of the low kissing number $k = 4$. The space group of the crystal is $P2_12_12$. Again, one capsid is centred at the origin [Wyckoff position 2(a), with $z = 0$]. In the (a, b) plane each virion has four kissing points (along plane diagonals of the

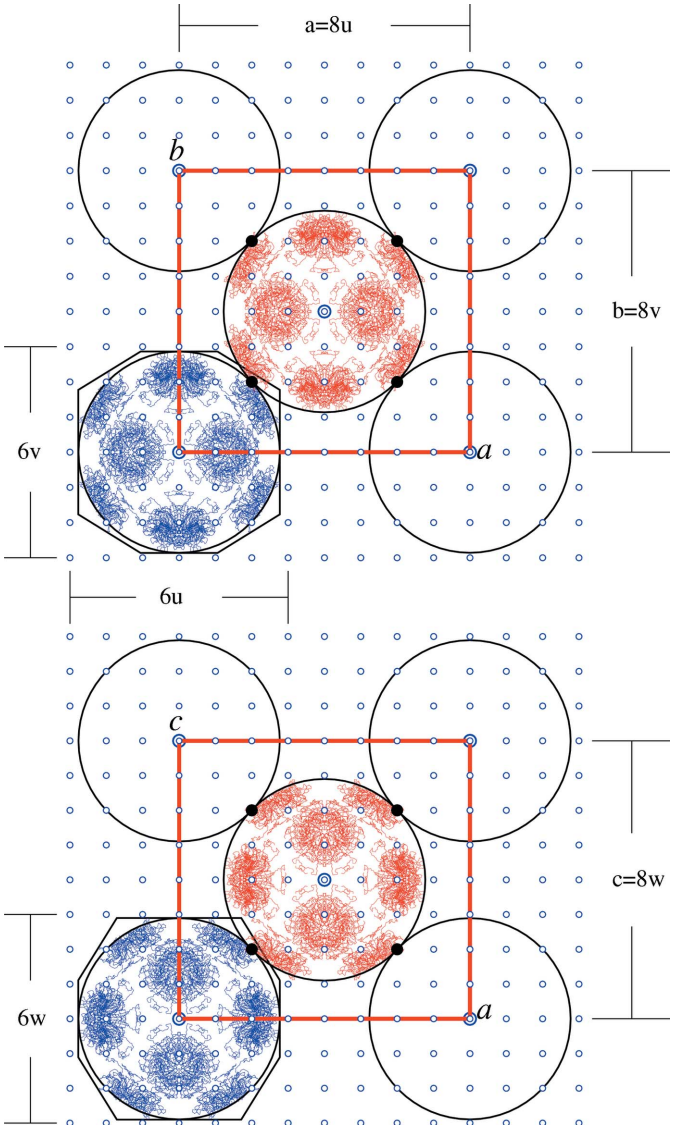

Figure 1
The orthorhombic crystal of the mengovirus shown as a packing of spheres inscribed in the ico-dodecahedra enclosing the capsid, in a projection along the c (top) and b (bottom) axes. The 12 kissing points (indicated by black filled circles) are at points of the packing lattice $\Lambda_P(u, v, w)$, which includes the crystal lattice $\Lambda(a, b, c)$ according to $a = N_a u$, $b = N_b v$, $c = N_c w$, with $N_a = N_b = N_c = 8$. The diameter of the packed spheres is approximately given by $6u = 6v = 6w$, so that the packing lattice is nearly cubic.

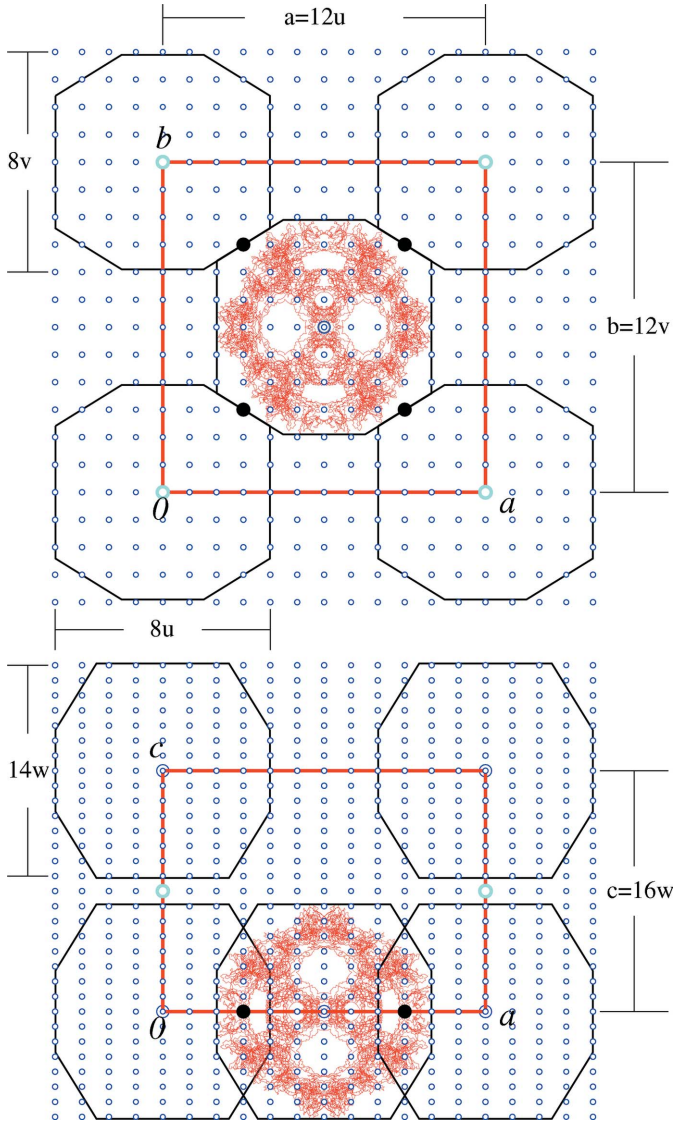

Figure 2
The orthorhombic crystal of the echovirus, type 1, is built from planes of tightly packed capsids, stacked along the c axis. Their interseparation is $2w = c/8$ with w and c the lattice parameters of the packing lattice $\Lambda_P(u, v, w)$ and of the crystal lattice $\Lambda(a, b, c)$, respectively. The interspacing of the enclosing ico-dodecahedra along the a and b axes is given by $4u = a/3$ and $4v = b/3$, respectively, ensuring the existence of four kissing points for each capsid at lattice points of Λ_P. The missing kissing points between the virions stacked along the c axis are also indicated.

unit cell), at the Wyckoff 4(c) positions with $z = 0$ and $x = y = 1/4$, $x = \bar{y} = 1/4$, respectively. Along the a axis the virions are separated by $4u = a/3$, and along b by $4v = b/3$. The viruses are stacked in the direction of the c axis with a distance between planes of $2w = c/8$, so that the expected kissing points at $z = 1/2$ are missing (Fig. 2). Summarizing, one has $N_a = N_b = 12$, $N_c = 16$, $n_a = n_b = 4$ and $n_c = 7$. The deviations of the real crystal from the ideal one, expressed in the lattice parameter ratios, are $a/b = 1$ (0.977), $b/c = 21/16 \simeq 1.312$ (1.370), $a/c = 21/16 \simeq 1.312$ (1.340), with the experimental values in parentheses.

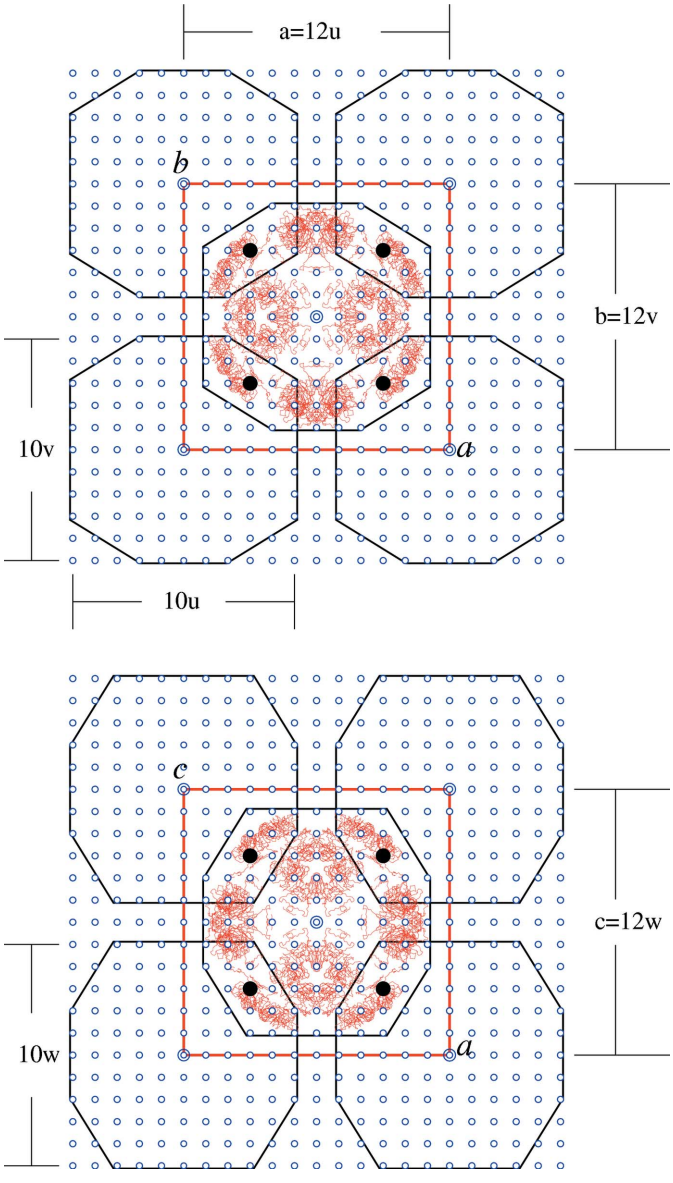

Figure 3
The packing of ico-dodecahedra enclosing the FMDV, serotype O, shown in similar projections as in the previous figures, fits very well with the cubic packing lattice $\Lambda_P(u)$, related to the crystal lattice $\Lambda(a)$, also cubic, by $a = 12u$. The filled dots of Λ_P mark the position of the eight kissing points, as one sees from the other projections adopted in Fig. 4.

3.4. The foot-and-mouth disease virus, strain O1

The crystal of the foot-and-mouth disease virus (FMDV), strain O1 BFS 1860 (1BBT; Fry *et al.*, 1993), is cubic with space group $I23$. The packing lattice, obtained from the crystal lattice Λ by the values $N_a = N_b = N_c = 12$ and $n_a = n_b = n_c = 5$, fits very well with the ico-dodecahedral enclosing forms having the icosahedral parameter $a_0 = 91$, as shown in Fig. 3, and with the packing of equal spheres with radius $R_0 = \tau a_0 = 147.2$ Å [with τ the golden number $(1 + 5^{1/2})/2$], inscribed in the corresponding icosahedral forms (Fig. 4). The eight kissing points of each capsid are at the Wyckoff position 8(c) with $x = 1/4$.

3.5. The foot-and-mouth disease virus A 10_{61} and the echovirus 11

The crystals of the FMDV, serotype A 10_{61} (1ZBE; Fry *et al.*, 2005), and of the echovirus type 11 (1H8T; Stuart *et al.*, 2002) have the hexagonal space-group symmetry $H3$ and $H32$,

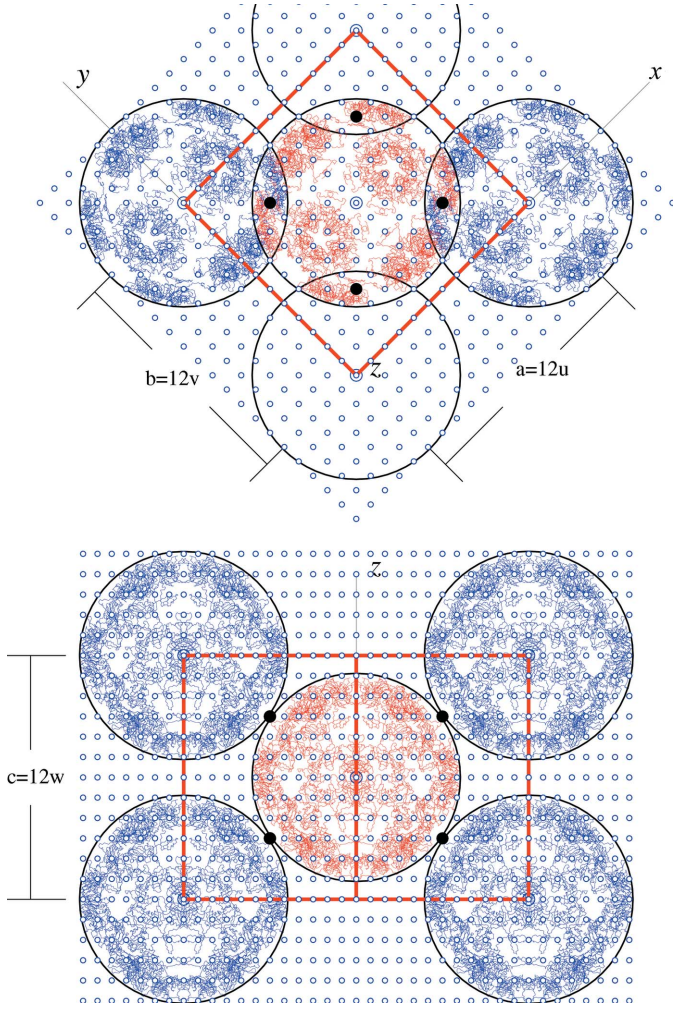

Figure 4
The same packing and crystal lattices of the FMDV O of Fig. 3 are plotted in alternative projections and with spherical enclosing forms in order to show explicitly that the kissing points are indeed there where the spheres touch.

Table 4
Contact sites of picornaviruses.

PDB key	Virus name and serotype	Indexed contact sites	Contact residues of the coat proteins			
			VP1	VP2	VP3	VP4
1BBT	FMDV O1	A = [333]		Thr191	Asp116	
1ZBE	FMDV A	A = [300], B = [330]	Thr133	Lys217, Glu218	Glu131	
		C = [214]	Ala110		Asp9	
1FMD	FMDV C	A = [333]		Thr191	Asp116, Lys193	
2PLV	Polio 1	A = [233]		Ser241	Ser203	
1EAH	Polio 2	A = [440]	Ala150			
		B = [404]	Ala291	Asn63	Tyr178	
1PVC	Polio 3	A = [575]		Gln240	Ser203	
1Z7S	Coxsackie A21	A = [444]		Ala241	Ser202	
1COV	Coxsackie B3	A = [024], B = [$0\bar{2}4$]		Asn28, Gly261	Thr143, Val146	
		C = [420], D = [$4\bar{2}0$]	Thr128			
		E = [404]	Gly82			
1MQT	Swine (∼B5)	A = [675]		Gly234	Ala203	
1OOP	Swine ukg/27/72	A = [336]		Thr233, Gly234	Ala202	
1EV1	Echo type 1	A = [330]		Gly74		
1H8T	Echo type 11	A = [300], B = [330]	Pro287	Asn161	Ala139	
		C = [214]	Asp136		Asn11	
1AYM	Rhinovirus 16	A = [334]		Asn233	Pro201	
4RHV	Rhinovirus 14	A = [330]	Asp91	Gly138	Thr231	
1RHI	Rhinovirus 3	A = [443]		Asn229	Gly203	
1FPN	Rhinovirus 2	A = [575]		Ser234	Pro203	
1R1A	Rhinovirus 1A	A = [423]	Val279		Thr92	
2MEV	Mengo	A = [220], B = [202], C = [022]	Phe104, Pro105	Lys162	Pro227, Ser229	Asn16
1TME	Theiler DA	A = [454]		Ser237	Gly203	
1TMF	Theiler BeAn	A = [222]	Pro271	Gly238, Thr237	Ser200, Thr204	
		B = [400]		Glu267		

respectively. These two cases are presented together because they are very similar. Up to a doubling of the structure along the hexagonal c axis (related to the additional twofold transformation in $H32$ with respect to $H3$) observed in the echovirus 11, the packing structure is practically the same (compare Fig. 5 and Fig. 6). The axial ratio c/a in the FMDV A is approximately $6^{1/2}$, which implies that the lattice is nearly face-centred cubic (f.c.c.). In a similar way, for the echovirus 11 it is $c/2$ which is approximately $6^{1/2}a$, so that now the hexagonal crystal lattice has a nearly f.c.c. sublattice. Up to this doubling of the unit cell, the packing parameters are correspondingly the same: $N_a = N_b = 6$ and $N_c = 24$ (FMDV A 10_{61}), $N_c = 48$ (echovirus 11), and $n_a = n_b = 3, n_c = 5$ in both cases. Note that the ideal axial ratio $a/c = 5/12$ indicated in Table 3 for the FMDV A 10_{61} is simply an approximation of $1/(6^{1/2})$, both ideal values ensuring that the crystal lattice is integral. The kissing number is $k = 12$, as in the cubic close-packed structure.

3.6. The coxsackievirus B3

The interest in this case is due to the low space-group symmetry of the crystal ($P2_1$) and the observed approximate $R32$ symmetry, which allows six possible monoclinic space-group settings, as discussed by Muckelbauer *et al.* (1995). From their investigation follows the location of the two capsids in the monoclinic unit cell (with unique axis b) at $x = y = 0, z = 1/4$ and $x = 1/2, y = 0, z = 3/4$ of the Wyckoff position 2(a). One then obtains the packing lattice, with packing parameters $N_a = N_c = 16$, $N_b = 8$ and $n_a = n_b = 4, n_c = 5$. The sphere enveloping the capsid, with radius $R_0 = 93.5\tau$ = 151.28 Å $\simeq b/2$, leads in the ideal case to the lattice parameter ratios $a/b = 2$ (1.902), $a/c = 5/4$ (1.102) and to the monoclinic angle β = 108.21 (107.70), where the experimental values are indicated in parentheses. In the ideal case, the monoclinic crystal lattice is integral.

4. Contact fingerprint diagrams and contact binding sites

Let us recall the basic ideas leading to a fingerprint diagram, as defined in Part II. The packing lattice allows a coarse-grained description of the capsid with indexed Cα residues of the four coat proteins. The indices are obtained from the integral approximation of the residue coordinates expressed on the basis of the packing lattice with the origin at the centre of a given capsid.

The enclosing forms of the virions meet at the kissing points of the crystal packing. For each coat protein of neighbouring capsids, the kissing-point-related (KPR) residues are those at minimal distance from a given kissing point. In particular, and in the packing lattice approximation of the KPRs, the *contact residues* are those sharing the same set of indices as a kissing point. The remaining ones are subdivided into *internal* and *external* according to whether they belong to the capsid at the origin, or to a neighbouring one, respectively. Of course not all icosahedral-equivalent contact sites are binding sites, because the kissing number is strictly smaller than 60. Therefore, the fingerprint diagram is defined by the KPR residues of the capsid in the packing-lattice approximation and at crystal space-group-equivalent positions and not according to

the icosahedral symmetry. In Part II, different fingerprint diagrams correspond to different serotypes of the rhinovirus. The question then arises whether this is also true for the *Picornaviridae* family.

Based on these ideas, the (contact) fingerprint diagrams of the selected picornaviruses listed in Table 1 have been derived. The result is summarized in Table 4 in terms of (indexed) contact sites and contact residues. Looking at this table, one verifies that no two fingerprint diagrams coincide, because their contact binding residues are different. This justifies the name 'fingerprint', at least for the picornaviruses selected. The property found in Part II for the rhinovirus is, therefore, also true for all the picornaviruses investigated so far: a different serotype implies a different contact fingerprint.

The differences observed can, however, be very subtle as shown here for a few examples. The two serotypes O1 and C of the FMDV have the same space-group symmetry $I23$, the same crystal-packing parameters (see Table 2) and nearly the same cubic lattice parameter: 345.0 and 347.6 Å, respectively. The indexed contact, internal and external sites and their residues are also correspondingly equal, up to one single contact residue (Lys193 of VP3) which only occurs in the serotype C, as indicated in Fig. 7 and in Table 4.

The fingerprint diagrams of two different virus species can also show minor differences only. The similarity between the FMDV, serotype A, and the echovirus 11 has already been underlined. Their fingerprint diagrams have correspondingly the same indexed positions, but the residues which occupy these sites are different (see Table 4). Fig. 8 shows the contact diagram of FMDV A.

It is also interesting to compare the pair poliovirus 3 and rhinovirus 2 (HRV2). Both viruses have the same space-group symmetry ($I222$) and the same packing parameters, doubled with respect to those used in the analysis of their crystal-packed structure in order to avoid kissing points with half-integer indices. They also have correspondingly the same contact sites of the two principal coat proteins VP2 and VP3,

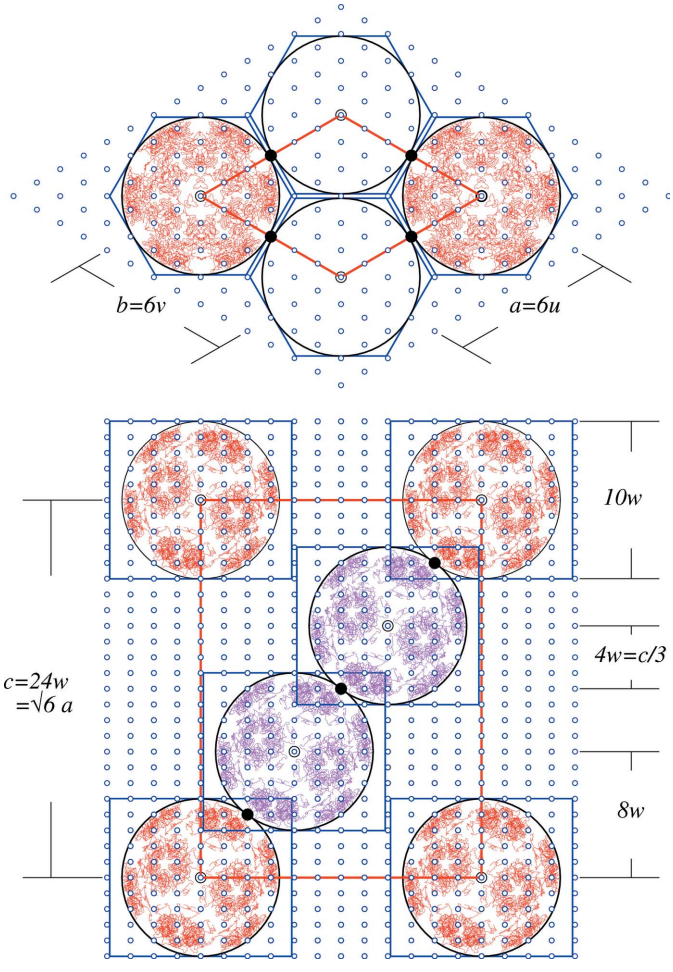

Figure 5
The packed structure of the hexagonal FMDV, serotype A, has a honeycomb arrangement in the (a, b) plane, stacked along the axial c direction with the same A, B, C sequence as in the cubic close packing of the enclosing spheres. The fitting of the packing lattice $\Lambda_P(u, v, w)$ is ensured by the (ideal) relations $a = b = 6u = 6v$ and $c = 24w \simeq a6^{1/2}$, so that Λ_P is f.c.c. to a good approximation. The black filled circles indicate kissing points.

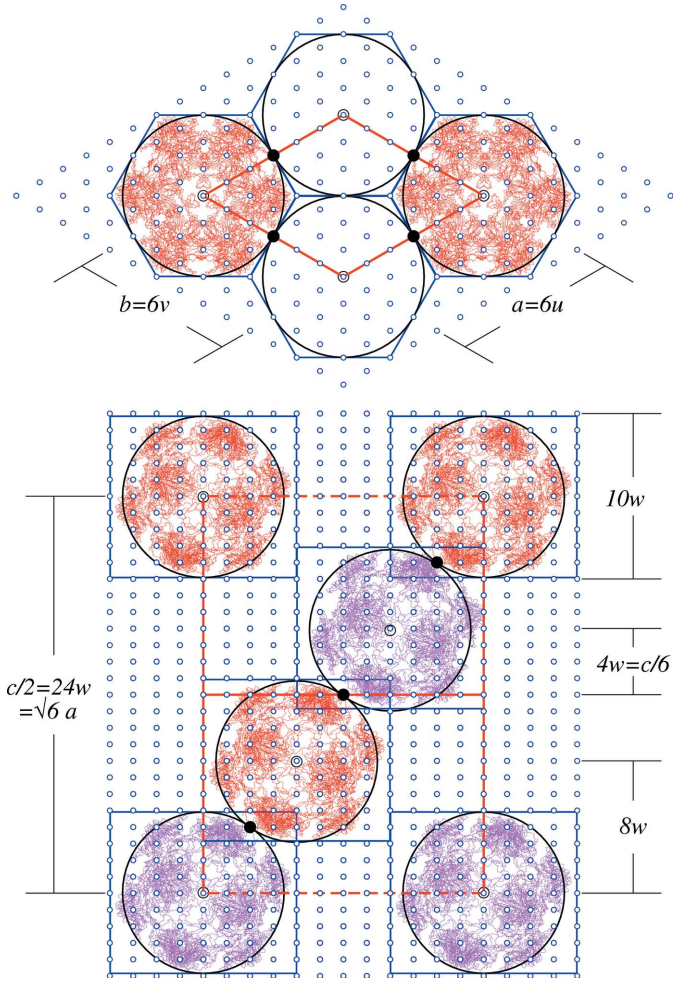

Figure 6
The crystal packing of the echovirus, type 11, is very similar to that of FMDV A, as one sees by comparison with the previous figure. The difference is restricted to a doubling of the unit cell, related to the different space-group symmetry ($H32$ instead of $H3$), so that one now has the (ideal) relation $c/2 = 24w = a6^{1/2}$.

but the residues are different and so also are their fingerprint diagrams. The one of HRV2 appears as Fig. 10 in Part II, and that of polio 3 is shown in Fig. 9.

5. Antigenic and receptor binding sites

As stated in §1, the second aim of the present Part III is the description of the antigenic and receptor binding sites of picornaviruses in a similar way as was done for the contact binding sites in the packing-lattice approximation, graphically plotted in corresponding diagrams. This is in order to recognize possible relations among the different binding sites.

Some general considerations are appropriate before moving to examples of antigenic and receptor fingerprint diagrams. The viral residue that interacts with a specific antibody defines an *epitope*. The corresponding antigenic site consists of contiguous (or overlapping) epitopes.

Some of the antigenic sites indicated in the literature are simply 'putative' or 'expected' ones. Others are derived from cross-checking in monoclonal antibody experiments, using specific antibodies obtained from special cultures (clones). Owing to the complexity of the conditions implying antibody binding, it is not surprising to find, for a given serotype, different lists of antigenic sites, depending on the author, with only a rough correspondence for the residues involved. The coarse-grained character intrinsic to a fingerprint diagram, where the indexed residues appear in the packing-lattice approximation, decreases this arbitrariness and is, therefore, appropriate to the situation.

Analogous considerations also apply to the receptor binding sites indicated in the literature, where sometimes the receptor is a specific one and sometimes only a member of a rich family of related proteins (as in the case of the immune globuline). An overview of the known molecular cell receptors, adapted from Rossmann *et al.* (2002), is given in Table 5.

The information contained in the fingerprint diagrams is characteristic for the virus considered (as suggested by the name 'fingerprint'), so that general trends only appear from the complete set of the various cases, despite the common

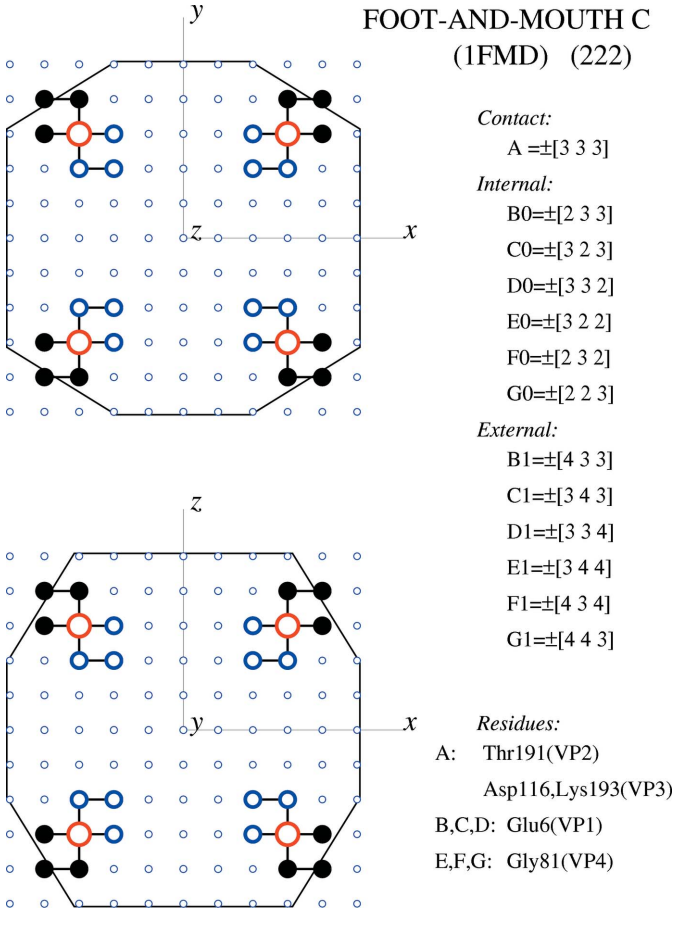

Figure 7
The two serotypes O and C of the FMDV have, correspondingly, the same indexed contact fingerprint diagram. The only difference is that in FMDV C (shown here) there is the additional contact residue Lys193 of the coat protein VP3, which is absent in FMDV O (not shown). Contact, internal and external residues are indicated by large open circles, small open circles and small filled circles, respectively.

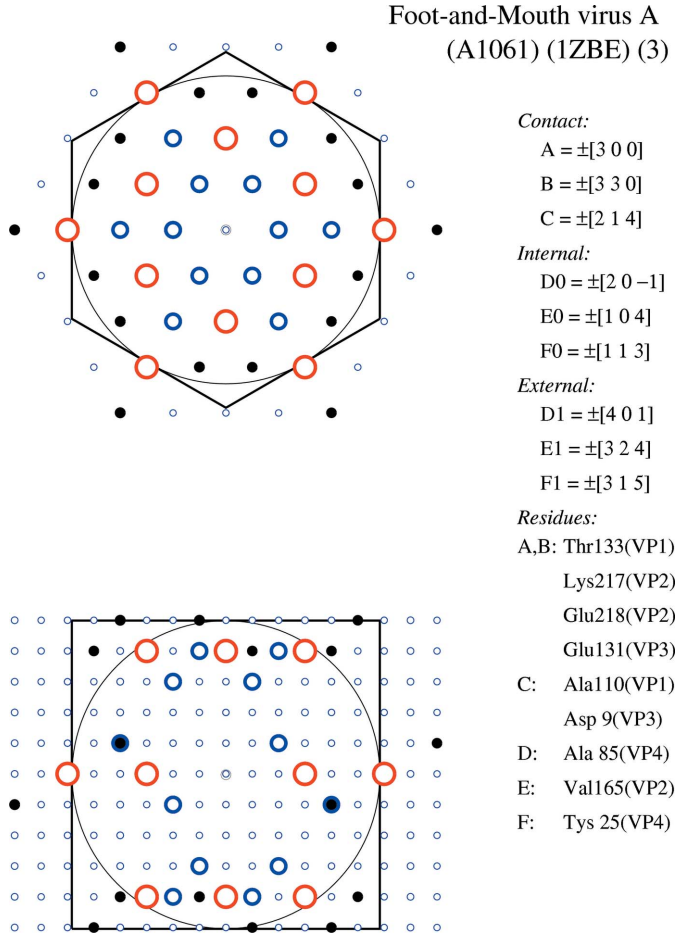

Figure 8
The contact fingerprint diagram of the FMDV, serotype A, has correspondingly the same KPR indexed positions (shown here) as the echovirus, type 11 (not shown), but the KPR residues are different. Note that both viruses have the same packed structure, as one sees from Figs. 5 and 6.

structural elements typical for the viruses belonging to the *Picornaviridae* family.

It is natural to associate the viral mutation, which allows the virus to reinfect the same host, with the variability in antigenic sites (as a reaction to the immune system) and the infection conservation with the receptor sites, where the virus binds with a specific cell membrane protein, allowing entry in the host cell.

This point of view underlies the 'canyon hypothesis', according to which conserved receptor sites are hidden in the canyon and protected from the sites where the antibodies bind (Rossmann & Palmenberg, 1988; Rossmann, 1989). In fact this hypothesis is not always verified. In particular, the cellular receptor of the human rhinovirus 2 binds around the fivefold axis and not in the canyon (Hewat *et al.*, 2000). Moreover, antibodies can also bind in the canyon (Smith *et al.*, 1996). Also not always true is the complementary view that different serotypes arise from the antigenic site variability. For example, the swinevirus occurs with one serotype only, despite the observed high genetic, antigenic and pathogenetic variability (Verdaguer *et al.*, 2003).

From all these observations the evidence emerges of a complex interplay between antigenic variation and receptor conservation. In all cases these binding sites involve residues at highly variable and exposed loops, as a result of the mutual interaction of the coat proteins. Therefore, conservation and mutations cannot simply be reduced to a dualistic dilemma for the virus in the selection between antigenic and receptor sites (Colman, 1997). Contact binding sites occur at the same exposed loops and apparently are also involved in the sophisticated structural properties of the capsid surface. It is, therefore, meaningful to explore the possible connections by adopting a common description: that of fingerprint diagrams.

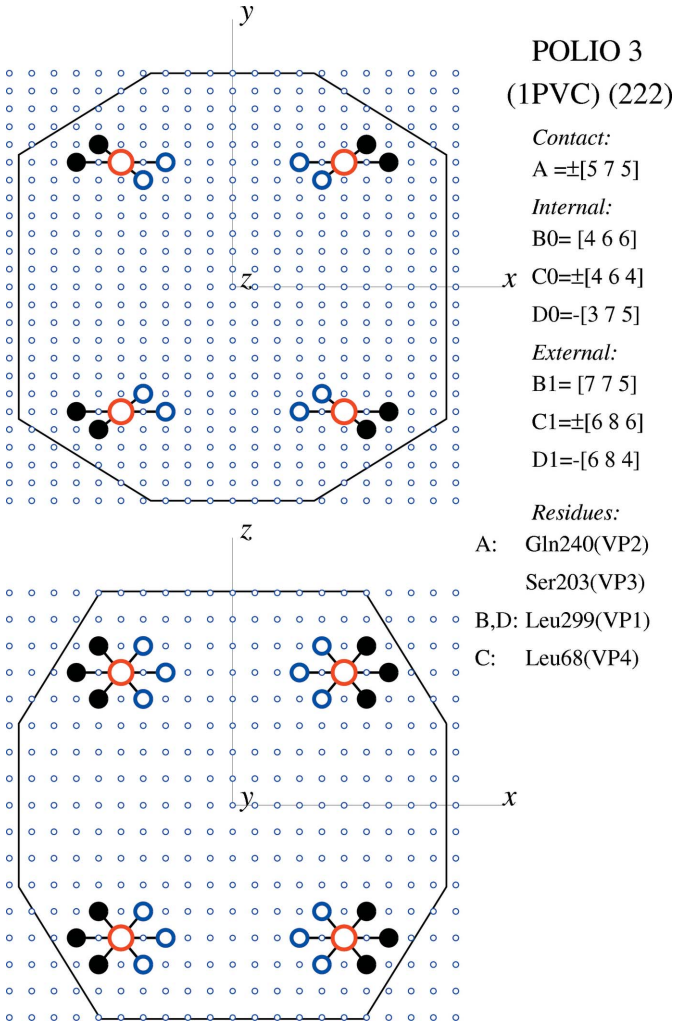

Figure 9
Shown is the contact fingerprint diagram of the poliovirus, type 3, which has the same KPR positions as the rhinovirus HRV2 (see Fig. 10 of Part II). The crystals of both viruses have the same space-group symmetry *I*222 and the same set of packing parameters (doubled with respect to those of the packed structure). Their contact fingerprint diagrams are, however, different.

6. Antigenic and receptor fingerprint diagrams

Antigenic and receptor sites are usually described in terms of *footprint diagrams* following the original ideas of Rossmann & Palmenberg (1988) and of Lee & Richards (1971), respectively, or alternatively by *roadmaps* of properties mapped on the surface of the viral capsid (Chapman, 1993).

A three-dimensional grid is considered with the origin at the virus centre and orthogonal axes oriented as the icosahedral twofold axes. The residues are then assigned to grid points (usually spaced at 2 Å intervals) within a given radius r (say of 3.4 Å). The footprint corresponds to the area on the viral surface covered by the bound molecule (antibody or receptor) and this justifies the name.

Here the role of the grid is taken over by the packing lattice considered in the previous section. As indicated in Table 3, the typical lattice parameter varies between 20 and 50 Å, so that instead of having one or more grid points for one atomic position, one or more residues are assigned to their nearest lattice point. One then obtains a coarse-grained description of the coat proteins, as done in Part II for the KPR residues, which (we recall) are defined by the Cα positions of the four coat proteins at minimal distance from the kissing points and include the contact residues in particular. Instead of a roadmap for viral surface properties and a footprint which takes into account the icosahedral symmetry of the capsid, one gets a *fingerprint* diagram, defined on points of a lattice invariant with respect to the space group of the crystal. The idea behind the name is that a fingerprint should allow the identification of the individual virus, including serotype and strain. But this is not the main reason for introducing a different diagrammatic characterization of these sites from the ones one finds in the literature. The relevant reasons are given in the next section.

The procedure used for the KPR residues is also applied to the antigenic and receptor sites, in terms of corresponding fingerprint diagrams, in order to get a description common to the three binding sites. In Table 6 the characteristic properties of a footprint are compared with those of a fingerprint diagram.

Table 5
Serotypes and receptors of picornaviruses.

Virus name	Short	Serotypes/strains	Molecular receptors
Foot-and-mouth disease virus	FMDV	A, O, C, Asia, Sat1, Sat2, Sat3	Integrin ($\alpha_v\beta_3$, $\alpha_v\beta_6$), heparin disaccharide, heparan sulfate (HS)
Human poliovirus	PV	PV1/Mahoney, PV2/Lansing, PV3/Leon, PV3/Sabin	Poliovirus receptor (PVR), integral membrane protein of the immunoglobulin superfamily
Coxsackievirus B	CVB	CVB1–CVB6	Coxsackievirus adenovirus receptor (CAR), decay-accelerating factor (DAF)
Coxsackie A virus	CAV	CAV1–CAV23	
		CAV9	$\alpha_v\beta_3$ Integrin
		CAV21	Intercellular adhesion molecule 1 (ICAM-1)
Swine vesicular disease virus	SVDV	Mutation from coxsackie B5 virus	CAR binding (putative), HS binding (putative)
Echovirus	ECHO	ECHO1–ECHO32	
		ECHO6, ECHO7	Decay-accelerating factor (DAF)
		ECHO1, ECHO8	$\alpha_2\beta_1$ Integrin (VLA-2)
Human rhinovirus	HRV	More than 100 serotypes	
		Major group (91) (HRV16, HRV14, HRV3)	ICAM-1
		Minor group (10) (HRV2, HRV1A)	Low-density lipoprotein receptor (LDL-R)
Mengo virus		Single serotype	
Theiler murine encephalomyelitis	TMEV	Theiler original group (TO/DA, TO/BeAn)	Sialic acid
		Theiler virulent group (GDVD, FA)	

Table 6
Comparison between footprint and fingerprint diagrams.

	Footprint	Fingerprint
Symmetry	Icosahedral point group	Crystal space group
Selected coat proteins	In a given fundamental region	Nearest to a given kissing point
Lattice/grid	Cubic grid ($\simeq$ 2 Å spaced)	Packing lattice ($\simeq$ 20–50 Å spaced)
Orientation	Orthogonal axes parallel to icosahedral twofold axes	As the crystal lattice (which is a sublattice)
Origin	Centre of the capsid	Centre of the capsid
Coarse graining	Residues assigned to grid points within a radius r ($\simeq$ 3.4 Å)	Residues assigned to their nearest lattice point (indexing)
Atomic positions	One or more grid points for one atomic position	One or more atomic positions for one lattice point
Idea behind the name	Surface area covered by the molecule bound to the capsid	Should allow the identification of the virus involved

To begin with, the antigenic and receptor sites collected from the literature for a number of picornaviruses are summarized in Table 7, together with the references where one finds the list of antigenic and receptor residues involved, all belonging to the three major proteins of the capsid.

Antigenic and receptor fingerprint diagrams, plotted side by side, have been derived for nine picornaviruses. In these diagrams, as in Table 7, the selected kissing point (and thus the corresponding contact site) is also indicated. As expected from the contact fingerprints, each antigenic and each receptor diagram is different, at least for the picornaviruses investigated so far.

Even in the case when antigenic and receptor residues are correspondingly the same, as for the rhinovirus 14 and 3 of the major group, their diagrams are different, as shown in Fig. 10 for HRV14 and in Fig. 11 for HRV3.

Worthy to be compared, for the same reasons as for their contact diagrams, are the fingerprints of the two serotypes of the FMDV: O1 (Fig. 12) and C (Fig. 13). While the antigenic diagrams are similar, their receptor fingerprints are not, for the simple reason that the G–H loop of the VP1 coat protein of FMDV C (residues 133–156) is disordered in the crystal, so that the coordinates of the receptor residues remain unknown. For the pair FMDV A and echovirus 11, which have correspondingly the same set of indices in the contact fingerprint (see Table 4), only the antigenic and receptor fingerprints of FMDV A can be shown (Fig. 14), because the interaction of echoviruses with the host cell is complex and not well understood (Semler & Wimmer, 2002).

Finally, the two viruses poliovirus 3 and rhinovirus 2, which share space-group symmetry (*I*222) and packing parameters, have not only different contact fingerprints (as already noted in §4), but also unlike antigenic and receptor diagrams (see Fig. 15 and Fig. 16). In particular, their receptor residues are different.

7. Why receptor and antigenic fingerprint diagrams

Despite the formal possibility for picornaviruses to extend the fingerprint diagrams, originally derived from contact points in crystal-packing structures, to receptor and antigenic sites, these extensions appear at first superfluous and not natural: superfluous because in the literature a diagrammatic characterization already exists for receptor/antigenic sites and not natural because there is no apparent reason to associate the existence of these sites to the ability of a virus to crystallize, as pointed out by one referee.

The rationale of a fingerprint extension to receptor/antigenic sites in *Picornaviridae* is based on properties observed in rhinoviruses which cannot be considered as accidental. In

particular, their structural properties depend on the two relevant symmetry groups involved. Those associated with the icosahedral symmetry of the capsid have been shown to be serotype independent (Janner, 2006*a*), whereas space-group dependence of the serotype is not only observed but also analysed in terms of fingerprint diagrams relating the crystal packing with an encoding of space-group elements in the capsid itself (Janner, 2010*b*).

Even if, in general, not clearly understood, there is certainly a relation between serotype and receptor/antigenic binding site variability. Therefore, one can safely suppose that in picornaviruses such correlation can be better analysed by taking the space-group symmetry into account rather than the icosahedral one. This is exactly what justifies the use for the various binding sites of fingerprints, which are space-group invariant.

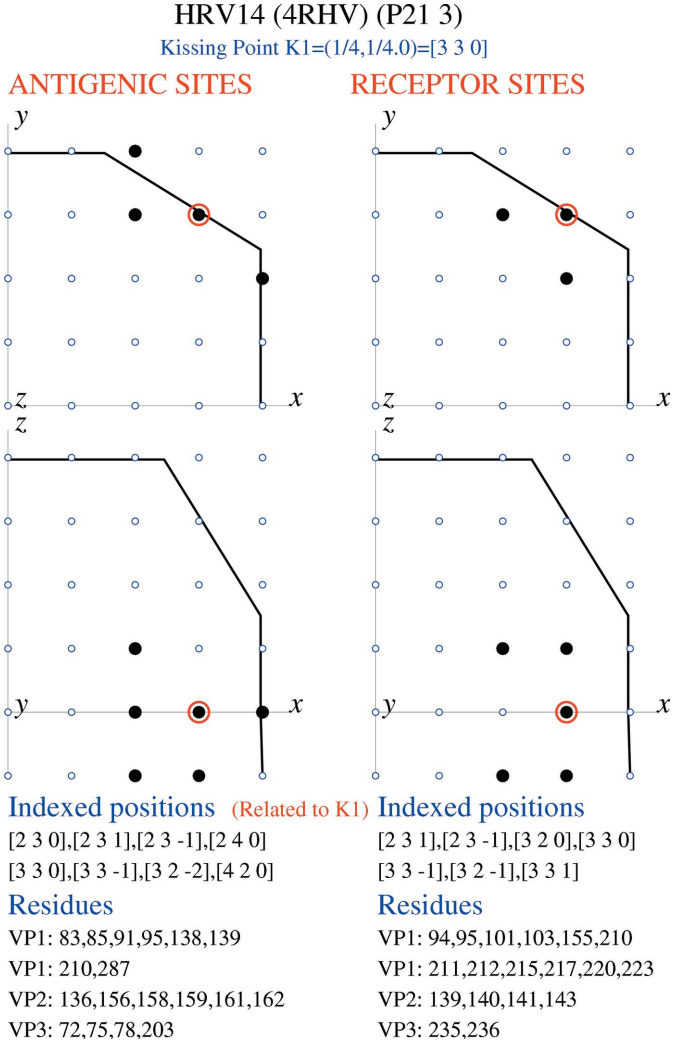

Figure 10
Shown are the antigenic and receptor fingerprint diagrams of the rhinovirus 14, with indexed residues belonging to the coat proteins with residues at minimal distance from the chosen kissing point *K*1 at the (1/4, 1/4, 0) position in the unit cell (with the indices [330] in the packing lattice). The antigenic and receptor residues of HRV14 and HRV3 are the same (both HRV14 and HRV3 belong to the same major group), but their fingerprint diagrams are different, as one sees by comparison with Fig. 11.

Moreover, these sites are surface effects connected with variable loops of the capsid proteins, which also play a role in the packing. The possibility of associating specific residues to a given fingerprint (listed in the figures presented in the paper) allows one to verify the role of the surface loops for each distinct binding site. The identification of these residues also permits inclusion in the analysis of biochemical properties and the geometry of the mutual positions.

On the basis of the observations quoted above, one may hope to arrive at an interpretation of the space-group dependence of these sites and of that of the serotype. One way towards this goal is to look at the space-group-invariant distribution of receptor and antigenic sites according to their fingerprint diagrams, as suggested by one of the referees.

8. Concluding remarks

The choice of the *Picornaviridae* family as a working field for the exploration, from a crystallographic point of view, of basic

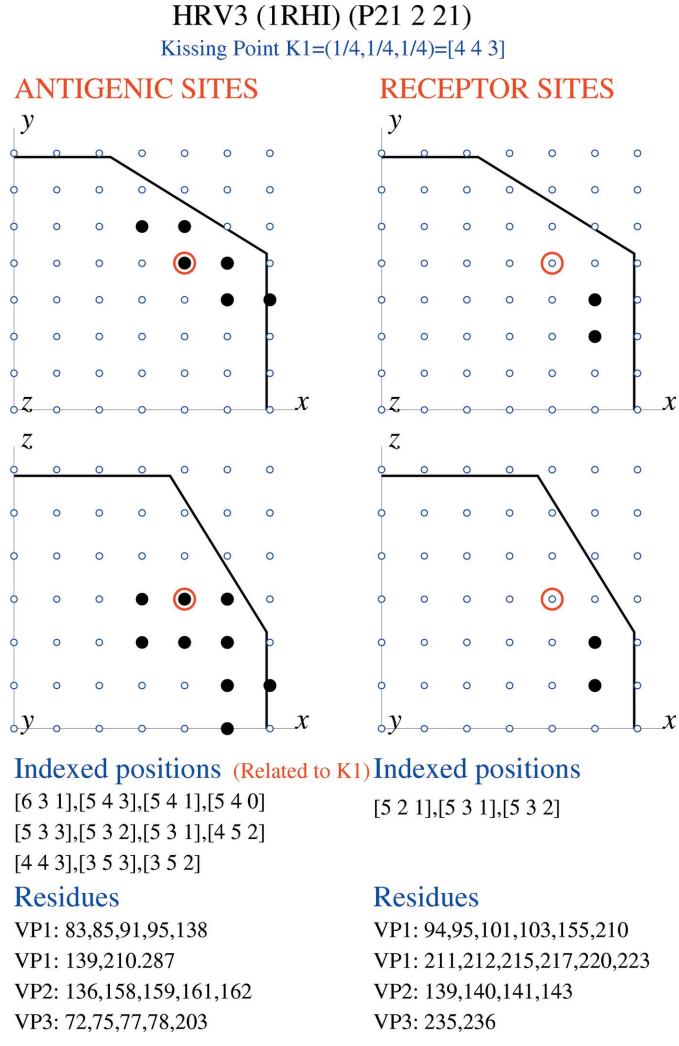

Figure 11
The antigenic and receptor fingerprint diagrams for the rhinovirus HRV3, which shares the same set of residues as HRV14, but has a different fingerprint (see Fig. 10).

Table 7
Antigenic and receptor binding sites.

PDB key/antigenic/receptor/references	Coat protein	Virus serotype/residues	Kissing point K_n/indexed positions
1BBT		FMDV O1	$K1$ = (1/4, 1/4, 1/4) = [333]
Antigenic	VP1	144, 147, 148, 149, 154,	Disordered G–H loop
Kitson *et al.* (1990)	VP1	43–45, 48, 208	[314], [214], [313]
Crowther *et al.* (1993)	VP2	70–73, 75, 77, 131, 134	[333], [334], [324], [224]
	VP3	56, 58	[323]
Receptor	VP1	193, 195	[314], [324]
Fry *et al.* (1999)	VP2	134, 135, 138	[324], [323]
Fry *et al.* (2005)	VP3	56, 58, 87, 88	[323]
1ZBE		FMDV A	$K7$ = (2/6, 1/6, 1/6) = [214]
Antigenic	VP1	142, 144, 146, 147, 148, 149–153, 154,	Disordered G–H loop
Kitson *et al.* (1990)	VP1	43–45, 48, 169, 204, 208	[204], [214], [114]
Fry *et al.* (2005)	VP2	70–73, 75, 77, 80, 134, 196	[105], [005]
	VP3	56, 58–61, 69, 70, 136, 139, 195	[104], [1$\bar{1}$4]
Receptor	VP1	193	[115]
Fry *et al.* (2005)	VP2	134, 135	[105]
	VP3	56, 88	[104]
1FMD		FMDV C	$K1$ = (1/4, 1/4, 1/4) = [333]
Antigenic	VP1	136–150,	Disordered G–H loop
Lea *et al.* (1994)	VP1	192–209	[324], [314], [323], [313]
	VP2	72, 74, 79	[323], [324], [224]
	VP3	58	[323]
Receptor	VP1	141–143	Disordered G–H loop
Verdaguer *et al.* (1995)			
2PLV		Polio 1	$K1$ = (1/4, 1/4, 1/4) = [233]
Antigenic	VP1	221–226	[143]
Page *et al.* (1988)	VP2	164–170, 270	[143]
	VP3	58–60, 71, 72, 73, 76	[133], [134], [233], [223]
Receptor	VP1	166–169, 214, 224–226,	
Belnap *et al.* (2000)		234, 235, 293–297	[033], [143], [133], [134]
	VP2	138–142	[133]
	VP3	58–60, 182, 183	[133], [134], [233], [124]
1PVC		Polio 3	$K1$ = (1/4, 1/4, 1/4) = [575]
Antigenic	VP1	89–100, 141–152, 166,	[176], [076], [086], [186], [176], [177], [077],
Ferguson & Minor (1990)		220–222, 253, 286–290	[185], [275], [294], [285], [375], [376], [066]
	VP2	164–172, 270	[386], [385], [396], [395], [394]
	VP3	58–60, 70, 71, 76–79	[465], [466], [476], [565], [555], [556]
Receptor	VP1	166–169, 214, 224–226, 234, 235, 293–297	[185], [085], [086], [285], [295], [376], [366], [466]
Belnap *et al.* (2000)	VP2	138–142	[285]
	VP3	58–60, 182, 183	[466], [476], [356]
1MQT		Swine	$K1$ = (1/4, 1/4, 1/4) = [675]
Antigenic	VP1	83, 84, 258, 273	[1 11 4], [394], [485]
Verdaguer *et al.* (2003)	VP2	151, 153, 160, 163, 233	[556], [656], [557], [675]
	VP3	62, 63, 76, 235	[485], [575], [3 10 4]
Receptor	VP1	200, 210, 258, 266, 269	[4 10 3], [393], [394], [494], [495]
Verdaguer *et al.* (2003)	VP3	88, 92, 181	[375], [385]
4RHV		Rhinovirus 14	$K1$ = (1/4, 1/4, 0) = [330]
Antigenic	VP1	83, 85, 91, 95, 138, 139, 210, 287	[330], [420], [33$\bar{1}$], [32$\bar{2}$]
Zhao *et al.* (1996)	VP2	136, 156, 158, 159, 161, 162	[330], [230], [231]
Verdaguer *et al.* (2000)	VP3	72, 75, 78, 203	[230], [240], [23$\bar{1}$]
Receptor	VP1	94, 95, 101, 103, 155, 210, 211, 212, 215, 217, 220, 223	[330], [33$\bar{1}$], [23$\bar{1}$], [32$\bar{1}$], [320]
Zhao *et al.* (1996)	VP2	139, 140, 141, 143	[330], [331], [231]
	VP3	235, 236	[330]
1RHI		Rhinovirus 3	$K1$ = (1/4, 1/4, 1/4) = [443]
Antigenic	VP1	83, 85, 91, 95, 138, 139, 210, 287	[531], [631], [541], [540], [532], [452]
Zhao *et al.* (1996)	VP2	136, 158, 159, 161, 162	[532], [533], [543]
	VP3	72, 75, 77, 78, 203	[443], [353], [352]
Receptor	VP1	94, 95, 101, 103, 155, 210, 211, 212, 215, 217, 220, 223	[531], [521], [532]
Zhao *et al.* (1996)	VP2	139, 140, 141, 143	[532]
	VP3	235, 236	[531], [532]

Table 7 (continued)

PDB key/antigenic/receptor/references	Coat protein	Virus serotype/residues	Kissing point K_n/indexed positions
1FPN		Rhinovirus 2	$K1$ = (1/4, 1/4, 1/4) = [575]
Antigenic	VP1	85, 86, 92, 260, 262, 264, 265,	[186], [086], [275], [375],
Verdaguer *et al.* (2000)		267–269, 272, 274, 276, 278	[386], [376], [366], [466]
Appleyard *et al.* (1990)	VP2	159, 161, 163, 164, 214, 216, 238	[485], [395], [385], [284], [575]
	VP3	59, 64	[476], [475]
Receptor	VP1	85, 87, 88, 132, 224, 226, 228	[186], [086], [177], [077]
Verdaguer *et al.* (2004)			

relations between structure and biological properties appears to be a suitable one.

The main result of the present contribution is that for a virus the relevance of the crystal structure is not limited to the determination of the atomic coordinates. The packing approach, with kissing points between spherical viral forms, could be applied straightforwardly to the whole family of picornaviruses, allowing the derivation of packing lattices, which connect spherical and/or indexed icosahedral enclosing forms with the crystal-lattice periodicity.

The packing-lattice approximation of the atomic positions of the coat proteins (indexed accordingly) is a very coarse-grained description of the capsid, differing by more than a factor of ten (or even 20) in spacing with respect to the grid usually adopted in roadmap and footprint diagrams of anti-

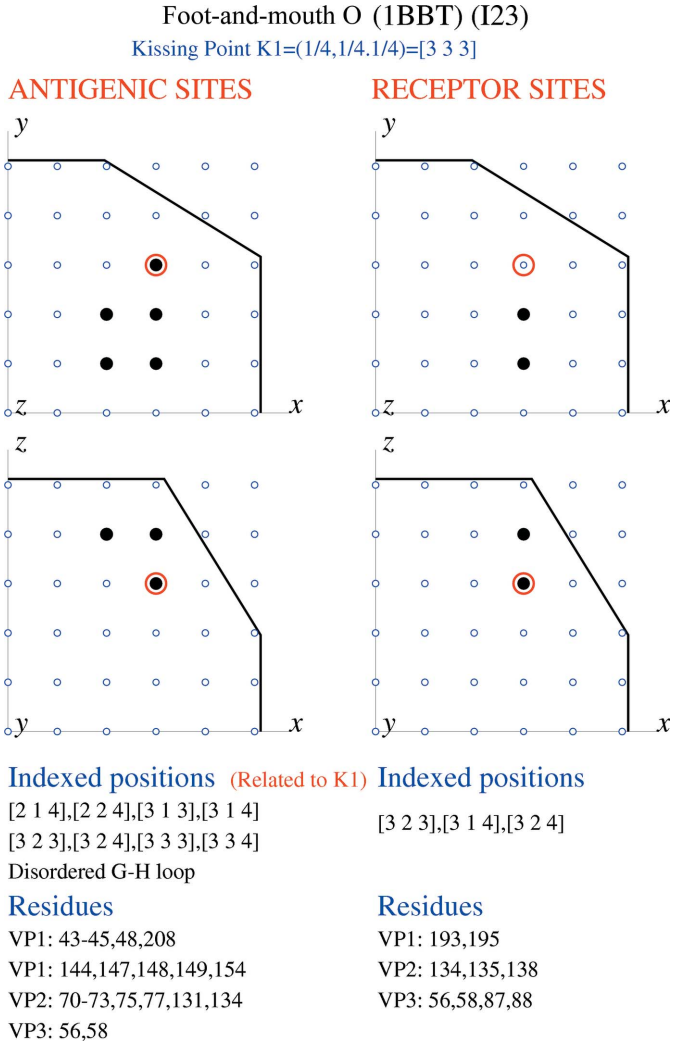

Figure 12
The antigenic fingerprint diagram of FMDV, serotype O, is similar to that for the serotype C (see Fig. 13); the two serotypes also have similar contact diagrams (as mentioned in the caption of Fig. 7).

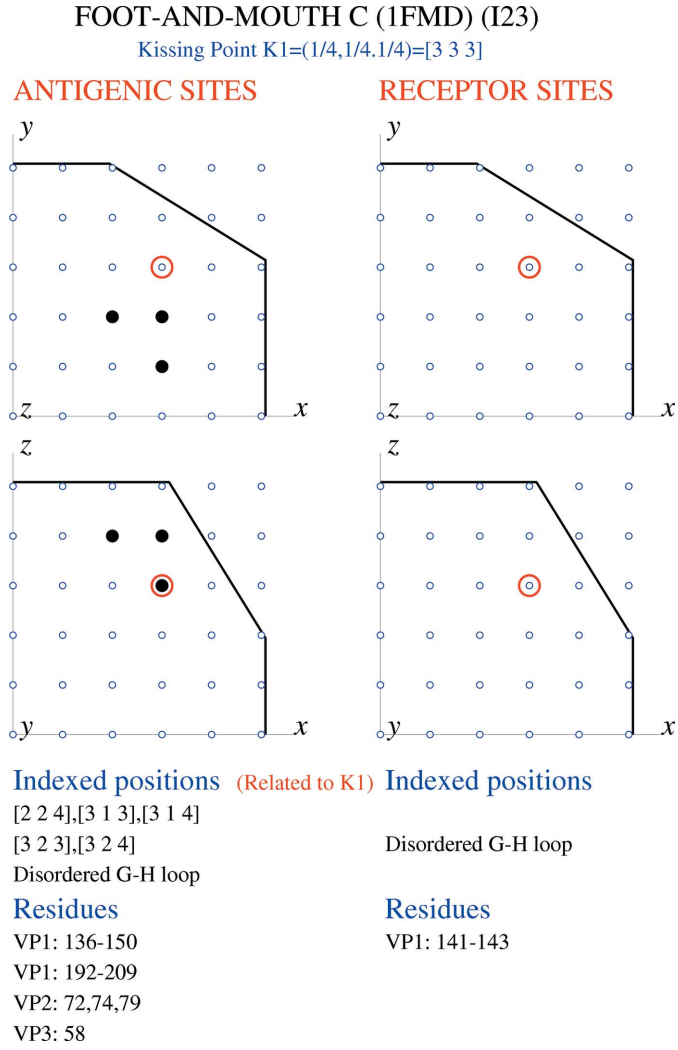

Figure 13
Shown is the antigenic fingerprint diagram of FMDV C. The receptor fingerprint is actually empty (only the chosen kissing point is indicated), because the receptor residues which belong to the G–H loop of the coat protein VP1 are disordered in the crystal.

genic and receptor binding sites, respectively. Despite the simplification of the alternative fingerprint diagrams because of the coarse graining, their specificity is apparently not lost. This has been verified for contact binding sites in 20 different strains of picornaviruses and for antigenic and receptor sites in about half as many cases.

The deeper connection between KPR residues and the crystal space-group symmetry revealed by the contact fingerprint diagrams, where the crystal structure is already encoded in the individual capsid (as discussed in Part II), has not been extended to the fingerprint diagrams of the antigenic and receptor sites. This is easily understandable. In order to include in the antigenic fingerprint diagram information on the pair of bound entities (capsid–antibody), one should first characterize the crystallographic properties of the antibody molecule involved and take these into account by the choice of a packing lattice adapted to both the capsid and the antibody enclosing forms. An antigenic fingerprint that includes this information is, in principle, possible but has not been done. Similar considerations also apply to the receptor fingerprint with respect to a given molecular receptor.

The various binding sites share common properties: they occur at (highly) variable surface loops, sometimes in complementary regions (like inside and outside the canyon), sometimes very nearby. Simple rules seem not to exist. In any case, one has to consider the whole. This is particularly true for the contact fingerprints where, in addition to the contact residues, one also has to include the so-called internal and external KPR residues of coat proteins, lying more inside the capsid.

A similar situation is likely to occur for a fourth set of binding sites, not considered in this paper: the antiviral binding site, where an antiviral compound, a drug (like the WIN compounds that are produced by Sterling Winthrop Inc., a pharmaceutical company in the USA) or a so-called pocket factor, is bound in an internal pocket of the capsid, in competition with receptor sites at the surface (Rossmann *et al.*, 2002; Hadfield *et al.*, 1995).

In conclusion, the present analysis is consistent with the view that the virus is a highly correlated complex system, requiring more than one approach for its unravelling.

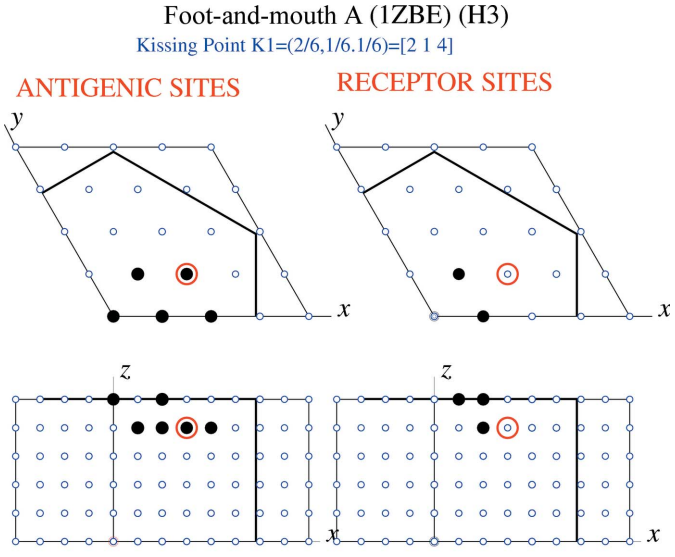

Indexed positions (Related to K1)
[0 0 5],[1 0 4],[1 0 5],[1 1 4]
[2 0 4],[2 1 4],[1 -1 4]
Disordered G-H loop

Residues
VP1: 43-45,48
VP1: 142,144,146,147,148
VP1: 149-153,154,169,204,208
VP2: 70-73,75,77,80,134,196
VP3: 56,58-61,69,70,136,139,195

Indexed positions
[1 0 4],[1 0 5],[1 1 5]

Residues
VP1: 193
VP2: 134,135
VP3: 56,88

Figure 14
For the pair FMDV A and echovirus type 11, which in their contact fingerprints have KPR residues with the same set of indices (indicated in Fig. 8 for the FMDV A), only the receptor diagram of FMDV A can be shown (together with the antigenic fingerprint) because there are no reliable data for the receptors of the echovirus owing to the complexity of the interaction between capsid and molecular receptor.

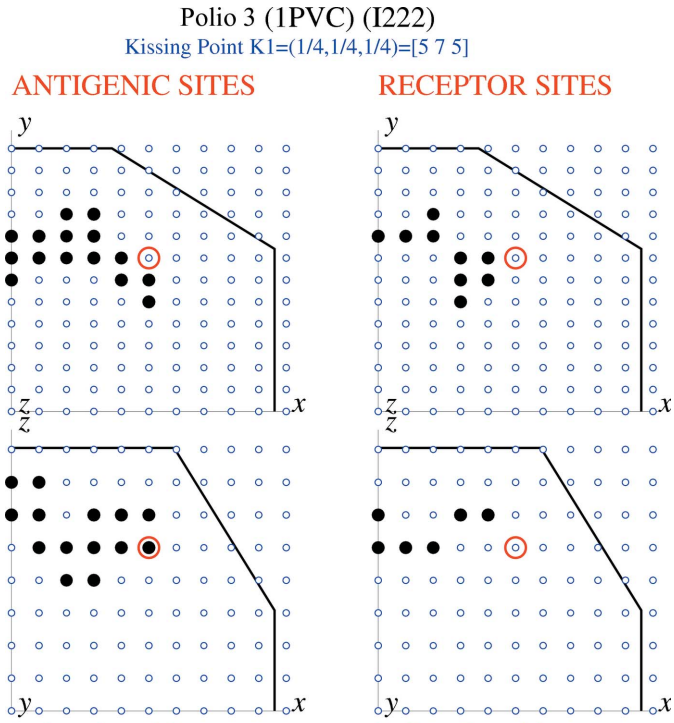

Indexed positions (Related to K1)
[0 6 6],[0 7 6],[0 7 7],[0 8 6],[1 7 6]
[1 7 7],[1 8 5],[1 8 6],[2 7 5],[2 8 5]
[2 9 4],[3 7 5],[3 7 6],[3 8 5],[3 8 6]
[3 9 4],[3 9 5], [3 9 6],[4 6 5],[4 6 6]
[4 7 6],[5 5 5],[5 5 6],[5 6 5]

Residues
VP1: 89-100,141-152,166
VP1: 220-223,253,286-290
VP2: 164-172,270
VP3: 58-60,70,71,76-79

Indexed positions
[0 8 5],[0 8 6],[1 8 5],[2 8 5]
[2 9 5],[3 5 6],[3 6 6],[3 7 6]
[4 6 6],[4 7 6]

Residues
VP1: 166-169,214,224-226
VP1: 234,235,293-297
VP2: 138-142
VP3: 58-60,182,183

Figure 15
The antigenic and receptor fingerprint diagrams of the poliovirus, type 3, are different from those of the rhinovirus 2 (shown in Fig. 16), even if the crystals of both viruses have the same space-group symmetry *I*222 and the same packing-structure parameters, as indicated in Table 2.

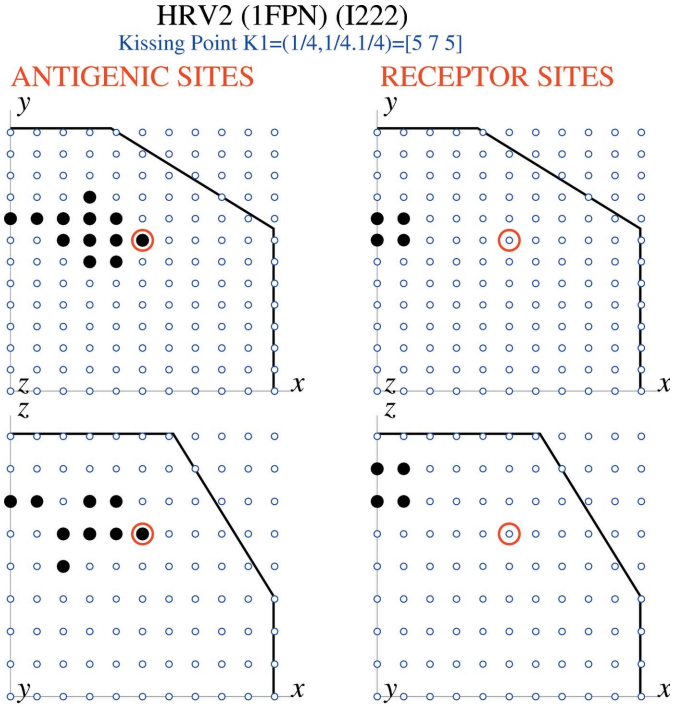

Figure 16
The antigenic and receptor fingerprints of the rhinovirus 2 (to be compared with those of the poliovirus 3 shown in Fig. 15).

Thanks are expressed to one of the referees for critical remarks allowing the improvement of the revised version and to the Editor for a number of text corrections.

References

Appleyard, G., Russel, S. M., Clarke, B. E., Speller, S. A., Trowbridge, M. & Vadolas, J. (1990). *J. Gen. Virol.* **71**, 1275–1282.
Arnold, E. & Rossmann, M. G. (1990). *J. Mol. Biol.* **211**, 763–801.
Belnap, D. M., McDermott, B. M. Jr, Filman, D. J., Cheng, N., Trus, B. L., Zuccola, H. J., Racaniello, V. R., Hogle, J. M. & Steven, A. C. (2000). *Proc. Natl Acad. Sci. USA*, **97**, 73–78.
Chapman, M. S. (1993). *Protein Sci.* **2**, 459–469.
Colman, P. M. (1997). *Structure*, **5**, 591–593.
Crowther, J. R., Farias, S., Carpenter, W. C. & Samuel, A. R. (1993). *J. Gen. Virol.* **74**, 1547–1553.
Ferguson, M. & Minor, P. D. (1990). *J. Gen. Virol.* **71**, 1271–1274.
Filman, D. J., Syed, R., Chow, M., Macadam, A. J., Minor, P. D. & Hogle, J. M. (1989). *EMBO J.* **8**, 1567–1579.
Filman, D. J., Wien, M. W., Cunningham, J. A., Bergelson, J. M. & Hogle, J. M. (1998). *Acta Cryst.* D**54**, 1261–1272.
Fry, E., Acharya, R. & Stuart, D. (1993). *Acta Cryst.* A**49**, 45–55.
Fry, E. E., Knowles, N. J., Newman, J. W. I., Wilsden, G., Rao, Z., King, A. M. Q. & Stuart, D. I. (2003). *J. Virol.* **77**, 5475–5486.
Fry, E. E., Lea, S. M., Jackson, T., Newman, J. W. I., Ellard, F. M., Blakemore, W. E., Abu-Ghazaleh, R., Samuel, A., King, A. M. Q. & Stuart, D. I. (1999). *EMBO J.* **18**, 543–554.
Fry, E. E., Newman, J. W. I., Curry, S., Najjam, S., Jackson, T., Blakemore, W., Lea, S. M., Miller, L., Burman, A., King, A. M. Q. & Stuart, D. I. (2005). *J. Gen. Virol.* **86**, 1909–1920.
Grant, R. A., Filman, D. J., Fujinami, R. S., Icenogle, J. P. & Hogle, J. M. (1992). *Proc. Natl Acad. Sci. USA*, **89**, 2061–2065.
Hadfield, A. T., Lee, W., Zhao, R., Oliveira, M. A., Minor, I., Rueckert, R. R. & Rossmann, M. G. (1997). *Structure*, **5**, 427–441.
Hadfield, A. T., Oliveira, M. A., Kim, K. H., Minor, I., Kremer, M. J., Heinz, B. A., Shepard, D., Pevear, D. C., Rueckert, R. R. & Rossmann, M. G. (1995). *J. Mol. Biol.* **253**, 61–73.
Hewat, E. A., Neumann, E., Conway, J. F., Moser, R., Ronacher, B., Marlovits, Th. C. & Blaas, D. (2000). *EMBO J.* **19**, 6317–6325.
Janner, A. (2004). *Acta Cryst.* A**60**, 198–200.
Janner, A. (2006*a*). *Acta Cryst.* A**62**, 270–286.
Janner, A. (2006*b*). *Acta Cryst.* A**62**, 319–330.
Janner, A. (2008). *Models, Mysteries and Magic of Molecules*, edited by J. C. A. Boeyens & J. F. Ogilvie, pp. 233–254. Dordrecht: Springer.
Janner, A. (2010*a*). *Acta Cryst.* A**66**, 301–311.
Janner, A. (2010*b*). *Acta Cryst.* A**66**, 312–326.
Kim, S., Smith, Th. J., Chapman, M. S. & Rossmann, M. G. (1989). *J. Mol. Biol.* **210**, 91–111.
Kitson, J. D. A., McCahon, D. & Belsham, G. J. (1990). *Virology*, **179**, 26–34.
Krishnaswamy, S. & Rossmann, M. G. (1990). *J. Mol. Biol.* **211**, 803–844.
Lea, S., Hernández, J., Blakemore, W., Brocchi, E., Curry, S., Domingo, E., Fry, E., Abu-Ghazaleh, R., King, A., Newman, J., Stuart, D. & Mateu, M. G. (1994). *Structure*, **2**, 123–139.
Lee, B. & Richards, F. M. (1971). *J. Mol. Biol.* **55**, 379–400.
Lentz, K. N., Smith, A. D., Geisler, Sh. C., Cox, S., Buontempo, P., Skelton, A., DeMartino, J., Rozhon, E., Schwartz, J., Girijavallabhan, V., O'Connel, J. & Arnold, E. (1997). *Structure*, **5**, 961–978.
Luo, M., He, C., Toth, K. S., Zhang, C. X. & Lipton, H. L. (1992). *Proc. Natl Acad. Sci. USA*, **89**, 2409–2413.
Muckelbauer, J. K., Kremer, M., Minor, I., Tong, L., Zlotnick, A., Johnson, J. E. & Rossmann, M. G. (1995). *Acta Cryst.* D**51**, 871–887.
Page, G. S., Mosser, A. G., Hogle, J. M., Filman, D. J., Rueckert, R. R. & Chow, M. (1988). *J. Virol.* **62**, 1781–1794.
Rossmann, M. G. (1989). *Viral Immunol.* **2**, 143–161.
Rossmann, M. G., He, Y. & Kuhn, R. J. (2002). *Trends Microbiol.* **10**, 324–331.
Rossmann, M. G. & Palmenberg, A. C. (1988). *Virology*, **164**, 373–382.
Semler, B. L. & Wimmer, E. (2002). Editors. *Molecular Biology of Picornaviruses.* Washington: ASM Press.
Smith, Th. J., Chase, E. S., Schmidt, T. J., Olson, N. H. & Baker, T. S. (1996). *Nature* (*London*), **383**, 350–354.
Stuart, A. D., McKee, Th. A., Williams, P. A., Harley, Ch., Shen, S., Stuart, D. I., Brown, T. D. K. & Lea, S. M. (2002). *J. Virol.* **76**, 7694–7704.
Verdaguer, N., Blaas, D. & Fita, I. (2000). *J. Mol. Biol.* **300**, 1179–1194.
Verdaguer, N., Fita, I., Reithmayer, M., Moser, R. & Blaas, D. (2004). *Nat. Struct. Mol. Biol.* **11**, 429–434.
Verdaguer, N., Jemenez-Clavero, M. A., Fita, I. & Ley, V. (2003). *J. Virol.* **77**, 9780–9789.
Verdaguer, N., Mateu, M. G., Andreu, D., Giralt, E., Domingo, E. & Fita, I. (1995). *EMBO J.* **14**, 1690–1696.
Xiao, C., Bator-Kelly, C. M., Rieder, E., Chipman, P. R., Craig, A., Kuhn, R. J., Wimmer, E. & Rossmann, M. G. (2005). *Structure*, **13**, 1019–1033.
Zhao, R., Pevear, D. C., Kremer, M. J., Giranda, V. L., Kofron, J. A., Kuhn, R. J. & Rossmann, M. G. (1996). *Structure*, **4**, 1205–1220.